Geophysical Journal (1989) **97**, 19–29

Comparison of iterative back-projection inversion and generalized inversion without blocks: case studies in attenuation tomography

Phyllis Ho-Liu, Jean-Paul Montagner and Hiroo Kanamori
Seismological Laboratory, California Institude of Technology, Pasadena, CA 91125, *USA*

Accepted 1988 July 21. Received 1988 May 31; in original form 1987 December 24

SUMMARY

Iterative back-projection tomography and generalized inversion without blocks ('no-block') are two different inversion techniques developed recently for 3-D studies, and are commonly applied to the inversion of travel-time data. In this study, we compare the two methods and derive one from the other under certain assumptions. We then apply these two methods to the attenuation problem, inverting for the quality factor, Q, of the medium. Usually, travel-time inversion involves large data sets and fine resolution is not possible if generalized inversion is applied. A relatively small data set with little redundancy enables us to apply both techniques with similar resolution. We applied the methods to the data sets obtained for two areas in southern California, the Coso–Indian Wells region and Imperial Valley. The results obtained by the two methods are very similar. Back-projection tomography is a direct and fast method for this type of problem. However, it does not provide formal error estimates and resolution. The no-block inversion requires more computational time, but formal errors and resolution can be directly computed for the final model. Thus, application of the two methods to the same data set enhances the objectivity of the final result.

Key words: attenuation, back-projection, generalized inverse, no-block inversion, tomography

1 INTRODUCTION

Geophysical problems often involve inversions of discrete data sets for unknown parameters of the earth. Many inversion algorithms have been developed solely for this type of problem. Pioneering work includes Backus & Gilbert (1968, 1970), Wiggins (1972), Franklin (1970) and Jackson (1979). More recent work in seismology includes Tarantola & Valette (1982) who applied a generalized inversion algorithm to solve non-linear and linear problems, and Comer & Clayton (1984), who used an iterative back-projection approach to solve linearized problems.

Many inversion techniques involve dividing a study area into blocks and inverting for unknown parameters such as slowness in each block. Tarantola & Valette's (1982) approach utilizes *a priori* information on the unknown parameters and inverts the data for unknowns without dividing the study area into blocks. In contrast, the back-projection approach iteratively back projects the data onto a model space composed of blocks. It processes the data set sequentially and thus can handle a large number of data points.

In this paper, we compare Tarantola & Valette's (1982) generalized inversion method and Comer & Clayton's (1984) iterative back-projection method using the same data set. We will refer to Tarantola & Valette's (1982) generalized inversion as the 'no-block inversion' or 'generalized inversion without blocks.'

2 INVERSE PROBLEM IN ATTENUATION TOMOGRAPHY

Many inversion methods in geophysics have been applied to travel-time data to invert for the velocity variations in a medium (Aki & Lee 1976; Chou & Booker 1979; Nercessian *et al.* 1984; Clayton 1984; Hearn & Clayton 1986a,b; Walck, 1988; Walck & Clayton 1988). Ho-Liu, Kanamori & Clayton (1988) applied a similar method to the amplitude data to determine S-wave quality factor, Q_β, of a medium.

Defining A_i as the observed amplitude, A_{oi} as the original amplitude of ray i, f as the frequency of seismic waves for the data set, Q as the quality factor of the medium, v as the velocity of the medium and $\mathbf{r}_i$ as the coordinates of ray i in vector form, we obtain

$$-\ln\left(\frac{A_i}{A_{oi}}\right) = \pi f \int_{L_i(v)} \frac{dl_i}{Q(\mathbf{r}_i)v(\mathbf{r}_i)}, \tag{1}$$

where $\int_{L_i(v)} dl_i$ denotes integration along ray i.

An analogy can be drawn at this point to the travel-time equation

$$t_i = \int_{L_i(s)} dl_i s(\mathbf{r}_i), \tag{2}$$

where t_i is the total travel time of ray i, s is the slowness of the medium and $\int_{L_i(s)}$ is the integration along the ray path L_i which depends on the slowness s.

In discrete form, equation (1) becomes

$$-\ln\left(\frac{A_i}{A_{oi}}\right)=\sum_{j=1}^{N}\pi f\frac{l_{ij}}{Q_j v_j}, \tag{3}$$

where l_{ij} is the length of the i-th ray in the j-th block, Q_j is the quality factor of the j-th block and v_j is the velocity of the j-th block and N is the total number of blocks in the model. A discrete form of equation (2) becomes:

$$\Delta t_i=\sum_{j=1}^{n_p}\Delta s_j l_{ij}, \tag{4}$$

where Δt_i is the residual in travel time for ray i, Δs_j is the differential slowness of the j-th block in the medium, and l_{ij} is the length of the i-th ray in the j-th block.

In the same way that we can directly invert Δt_i for Δs_j in equation (4), we can invert $-\ln\left(\frac{A_i}{A_{oi}}\right)$ for Q_j in equation (3), using a reference model for v_j.

Complications in the left-hand side of the above equations come from the initial source amplitudes, radiation pattern effects and emergence angles of P- and S-waves, and were discussed in Ho-Liu *et al.* (1988). In this paper, we focus on the application of the no-block inversion technique (Tarantola & Valette 1982) to the attenuation problem and its comparison with the back-projection inversion technique (Comer & Clayton, 1984). We will use the same assumptions as in Ho-Liu *et al.* (1988) in solving the problem. Estimation of the radiation pattern correction can be done using the first motion data, initial source amplitudes can be estimated from the P and SV velocities at the source, and the effect of emergence angles can be estimated by varying an uncertainty term in the method (Ho-Liu *et al.* 1988).

3 ITERATIVE BACK-PROJECTION TOMOGRAPHY

In iterative back-projection tomography, we solve a discretized problem in the form

$$d_i=\sum_j l_{ij}p_j, \tag{5}$$

where d_i is the data obtained for ray i, p_j is the unknown parameter for the j-th block, and l_{ij} is the length of ray i in the j-th block. Note that l_{ij} is zero for any block not crossed by ray i. The algorithm used in Ho-Liu *et al.* (1988) is the same as the algorithm described by Comer & Clayton (1984) or by Walck & Clayton (1988).

Each iteration in the calculation can be described by the following equations:

$$p_j^{(k+1)}=p_j^{(k)}+\frac{\sum_{i=1}^{n_d}\left(\frac{d_i^{(k)}}{L_i}\right)l_{ij}}{\mu+\sum_{i=1}^{n_d}l_{ij}} \tag{6a}$$

$$d_i^{(k)}=d_i^{(0)}-\sum_{j=1}^{n_p}l_{ij}p_j^{(k)}, \tag{6b}$$

where k denotes the index of iteration, L_i is the total length of ray i, and μ is a damping constant.

The above algorithm, with $\mu=0$, simply iteratively back projects the data onto each j-th block with an appropriate proportion. The proportion is determined by the ratio of the ray length of ray i in the j-th block to the total ray length L_i of rav i. The damping factor μ stabilizes the solution. For $\mu=0$, in case of small $\sum_i l_{ij}$, the value of $p_j^{(k+1)}$ will be large, and therefore less constrained. In order to reduce this effect, a damping constant is added to the iteration. Choice of the value of the damping constant depends on the data set and is often empirical. In general, the average of the total ray length through a block is chosen to be the value of the damping constant. In the two case studies to which we applied the back-projection inversion, we used a damping factor of 30. We will give a more intuitive meaning to this damping constant in the section where the two inversion methods are compared.

As was pointed out by Dines & Lytle (1979) and Comer & Clayton (1984), this algorithm is equivalent to a minimization of:

$$\sum_{i=1}^{n_d}\left(d_i^{(0)}-\sum_{j=1}^{n_p}l_{ij}p_j\right)^2\Big/L_i. \tag{6c}$$

This minimization implies that the shorter the path, the more weight the data carry. In other words, we know more about where the possible locations of the anomalies are for a shorter path.

In back-projection tomography, no matrix inversion is necessary, so we can use very small blocks (e.g. $2\times2\times1$ km).

The back-projection method was applied to two areas in southern California: the Coso–Indian Wells region and Imperial Valley (Fig. 1). Amplitudes of P- and S-waves were measured only on the vertical-component seismograms since horizontal instruments were not available. Sixteen earthquakes were chosen as the data set in the Coso study and fifteen earthquakes for the Imperial Valley area. These two data sets were selected so as to provide good azimuthal and depth coverage, while keeping the amount of computation to a reasonable level. Details are described in Ho-Liu *et al.* (1988) and will not be presented in this paper. Inversion results are presented in 1, 2 or 4 km thick depth slices (Figs 3a and 5a for Coso and Imperial Valley, respectively). All results were smoothed by a nine-point filter before presented, so the apparent maximum resolution is 6×6 km. In Figs 3 and 5, solid dots indicate attenuation anomalies. The size of the dots is proportional to the intensity of the anomalies. The scale is in $1/Q$. The attenuation was not determined for areas crossed by less than two rays. These areas remain blank in the figures.

In the back-projection method, since the inverse of the matrix associated with the equation $\mathbf{d}=L\cdot\mathbf{p}$ is not available, we cannot directly construct the classical resolution kernel or the covariance matrix for the model parameters. In order to assess the resolution of the inversion, one can calculate the resolving power of the technique for a data set generated by a synthetic point anomaly. This experiment gives the impulse response of the inversion through a numerical forward calculation. The effect of noise can be indirectly estimated by using random noise as input data. Results of the inversion should then give random parameter values. One can also infer the reliability

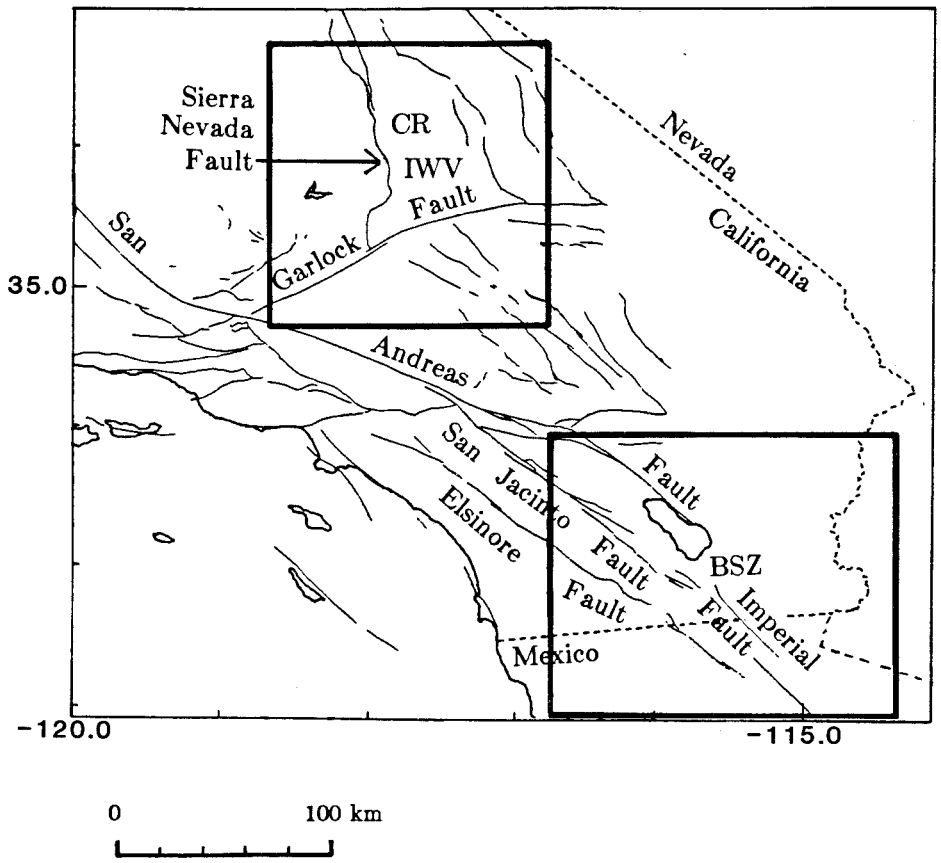

Figure 1. Boxes enclose the attenuation tomography study areas in Coso–Indian Wells Valley and Imperial Valley, southern California. Major faults are indicated and the abbreviations are: CR—Coso Range, IWV-Indian Wells Valley and BSZ—Brawley Seismic Zone.

of the results from the density of the hit-counts in the model. The denser the number of hits in an area, the more reliable the result. However, these numerical tests are indirect.

4 GENERALIZED INVERSION WITHOUT BLOCKS

Since the data sets used in this study are relatively small compared to many of those used in travel-time studies, we can apply the no-block inversion technique to them.

The quality factor, $Q(\mathbf{r})$, is now solved for in a continuous form (equation 1), where $\mathbf{r}$ denotes the position vector. We can solve the problem directly by the generalized inversion technique without blocks as described by Tarantola & Valette (1982).

This inversion technique is based on the assumption that we can estimate an *a priori* covariance function of the model parameters, C_{p^o}, and observed covariance function of the data, C_{d^o}. Here, following Tarantola & Valette (1982), we assume a Gaussian model parameter covariance function

$$C_{p^o}(\mathbf{r}, \mathbf{r}') = \sigma_p^2 \exp\left(-\frac{1}{2}\frac{|\mathbf{r}-\mathbf{r}'|^2}{L^2}\right), \tag{7a}$$

where L is the correlation length of the unknowns, σ_p is the *a priori* error in the model parameter. Since the data are discrete, C_{d^o} is a matrix. We assume that

$$[C_{d^o}]_{ij} = (\sigma_{d_{ij}})^2 \delta_{ij}, \tag{7b}$$

so that $[C_{d^o}]$ is a diagonal matrix with its diagonal terms equal to the variances, $\sigma_{d_i}^2$, of the data (no cross correlations in the data space). We also assume that the uncertainties in the data space are uncorrelated with the *a priori* uncertainties in parameter space ($C_{d^o p^o} = 0$).

Using these covariance functions, we solve equation (1) by the algorithm given by Tarantola & Nercessian (1984)

$$p^{k+1}(\mathbf{r}) = p^o(\mathbf{r}) + \pi f \sum_i W_i^k \int_{L_i(\mathbf{p}^k)} \frac{1}{v_i} dl_i C_{p^o}(\mathbf{r}, \mathbf{r}') \tag{8a}$$

$$W_i^k = \sum_j [(S^k)^{-1}]_{ij} V_j^k \tag{8b}$$

$$[S^k]_{ij} = (C_{d^o})_{ij} + \pi^2 f^2 \int_{L_i(\mathbf{p}^k)} \frac{1}{v_i} dl_i \int_{L_j(\mathbf{p}^k)} \frac{1}{v_j} dl_j C_{p^o}(\mathbf{r}_i, \mathbf{r}_j) \tag{8c}$$

$$V_j^k = d_j^0 - \pi f \int_{L_j(\mathbf{p}^k)} \frac{1}{v_j} dl_j p^o(\mathbf{r}_j) \tag{8d}$$

where $d_j^0 = -\ln\left[\frac{A_j}{A_{o_j}}\right]$ and $p(\mathbf{r}) = 1/Q(\mathbf{r})$.

The actual problem can be non-linear in the sense that the path in equation (1) depends on the velocity. Variations in velocity can yield variations in amplitude, but we assume that this effect is small enough that we can carry out the inversion using the initial reference velocity model or use

the tomographic velocity structures inverted from travel-time residuals. Therefore, we have a linear problem.

Since the inversion for $1/Q$ is linear, we do not have to iterate to obtain the final model, so we omit k in the equations. The *a posteriori* model covariance, $C_p(\mathbf{r}, \mathbf{r}')$, is computed by

$$C_p(\mathbf{r}, \mathbf{r}') = C_{p^o}(\mathbf{r}, \mathbf{r}') - \sum_i \sum_j \int_{L_i(p)} \frac{\pi f}{v} dl_i \int_{L_j(p)} \frac{\pi f}{v} dl_j C_{p^o}(\mathbf{r}, \mathbf{r}_i)[S^{-1}]_{ij} C_{p^o}(\mathbf{r}_j, \mathbf{r}'). \tag{9a}$$

The resolution is given by:

$$R(\mathbf{r}, \mathbf{r}') = \sum_i \sum_j \int_{L_i(p)} C_{p^o}(\mathbf{r}, \mathbf{r}_i) \frac{\pi f}{v(\mathbf{r}_i)} dl_i [S^{-1}]_{ij} \frac{\pi f}{v(\mathbf{r}')} dl_j(\mathbf{r}'). \tag{9b}$$

The calculation requires only inversion of an *nrays* × *nrays* matrix, where *nrays* is the number of rays in the data set and the most time consuming part is evaluation of the double integral in equation (8c). Since *nrays* is about 300 in our problem, this method can be used.

The choice of correlation length, L, depends on the resolution one wants to attain, under the condition that the area of interest is well resolved (that is, the error is smaller than the amplitude of the anomaly resolved). In the limit as $|\mathbf{r} - \mathbf{r}'|/L \to 0$ based on our *a priori* model covariance (equation 7a), or equivalently if we assume that $C_{p^o}(\mathbf{r}, \mathbf{r}') = \sigma_p^2 \delta(\mathbf{r}, \mathbf{r}')$, then we obtain the Backus & Gilbert (1970) type of generalized inversion with the 'trade-off' parameter, f, which is related to σ_p^2 in the form $1/\sigma_p^2 = f/(1-f)$. As $\sigma_p^2 \to \infty$, we invert the data with the maximum resolution, with most data explained by the resulting model and the least stability to noise in the data, as $\sigma_p^2 \to 0$, our results give the lowest resolution but most stable solution. However, the data are not well explained. Since the objective of this paper is to compare the iterative back-projection tomography to the no-block inversion, we will present only results with correlation lengths L that correspond to the resolution of the back-projection results.

5 APPROXIMATE FORM OF BACK-PROJECTION ALGORITHM

We now show that the algorithm of Comer & Clayton (1984), as given by equation (6a), can be approximated from the general algorithm of Tarantola & Valette (1982). Since Comer & Clayton use discrete blocks, we write the algorithm of Tarantola & Valette in discrete form and choose the form of generalized inversion given by Tarantola & Valette (1982), relating $p^{(k)}$ to $p^{(k-1)}$ where (k) is the index of iteration [equation 25 of Tarantola & Valette (1982)]. In discrete form, we have:

$$p_j^{(k)} = p_j^{(k-1)} + \sum_{n=1}^{n_p} [S^{-1}]_{jn} \sum_{i=1}^{n_d} \left\{ \frac{l_{in}}{\sigma_{d_i}^2} \left[d_i - \sum_{r=1}^{n_p} l_{ir} p_r^{(k-1)} \right] - \sum_{r=1}^{n_p} [C_{p^o}^{-1}]_{nr} (p_r^{(k-1)} - p_r^{(0)}) \right\}, \tag{10}$$

where $[S^{-1}]_{jn}$ is the jn-th element of the inverse of matrix S whose elements are s_{jn}:

$$s_{jn} = \sum_{m=1}^{n_d} l_{mj} l_{mn} \frac{1}{\sigma_{d_m}^2} + [C_{p^o}^{-1}]_{jn}.$$

Comer & Clayton (1984) minimize the norm given by equation (6c) and Tarantola & Valette (1982) minimize the norm $(\mathbf{d} - \mathbf{d}^o)^T C_d^{-1} (\mathbf{d} - \mathbf{d}^o) + (\mathbf{p} - \mathbf{p}^o)^T C_p^{-1} (\mathbf{p} - \mathbf{p}^o)$. Since only a small number of boxes are traversed by a single ray, the matrix L has sparsely distributed non-zero elements. The product $L^T L$ is consequently diagonally dominant. Then if we choose $[C_{p^o}^{-1}]_{jn} = \frac{1}{\sigma_p^2} \delta_{jn}$, we can approximate equation (10) by:

$$p_j^{(k)} \approx p_j^{(k-1)} + \frac{1}{s_{jj}} \sum_{i=1}^{n_d} \left\{ \frac{l_{ij}}{\sigma_{d_i}^2} \left[d_i - \sum_{r=1}^{n_p} l_{ir} p_r^{(k-1)} \right] - \sum_{r=1}^{n_p} [C_{p^o}^{-1}]_{nr} [p_r^{(k-1)} - p_r^{(o)}] \right\}. \tag{11}$$

We now drop the correction term $[C_{p^o}^{-1}](p_r^{(k-1)} - p_r^{(o)})$ in each iteration by assuming that in a linear problem, this correction around a reference point $p_r^{(o)}$ is negligible to the first order; hence, $p_r^{(k-1)} - p_r^{(o)} \to 0$. Equation (11) then becomes

$$p_j^{(k)} - p_j^{(k-1)} \approx \frac{\sum_{i=1}^{n_d} \frac{l_{ij}}{\sigma_{d_i}^2} \left(d_i - \sum_{r=1}^{n_p} l_{ir} p_r^{(k-1)} \right)}{\sum_{m=1}^{n_d} \frac{l_{mj} l_{mj}}{\sigma_{d_m}^2} + \frac{1}{\sigma_p^2}}. \tag{12}$$

For ray paths that are short relative to the block size, we can assume that $l_{mj} \approx L_m$, where L_m is the total ray length of ray m. Therefore, we have:

$$\sum_{m=1}^{n_d} \frac{l_{mj} l_{mj}}{\sigma_{d_m}^2} \approx \sum_{m=1}^{n_d} l_{mj} \frac{L_m}{\sigma_{d_m}^2}.$$

Equation (12) then becomes

$$p_j^{(k)} - p_j^{(k-1)} \approx \frac{\sum_{i=1}^{n_d} \frac{l_{ij}}{\sigma_{d_i}^2} \left(d_i - \sum_{r=1}^{n_p} l_{ir} p_r^{(k-1)} \right)}{\sum_{m=1}^{n_d} \frac{l_{mj} L_m}{\sigma_{d_m}^2} + \frac{1}{\sigma_p^2}}. \tag{13}$$

In equation (6a), we see that Comer & Clayton's algorithm applies a $1/L_i$ weighting to the data. In order to have the equivalent weighting, it is necessary to choose $\sigma_{d_m}^2 = \sigma_d'^2 (L_m/\Lambda)$, where σ_d' is the average error in data and Λ is a constant of normalization. Then we can write (13) in the form of Comer & Clayton's algorithm (1984):

$$p_j^{(k)} - p_j^{(k-1)} \approx \frac{\sum_{i=1}^{n_d} \frac{l_{ij}}{L_i} \left(d_i - \sum_{r=1}^{n_p} l_{ir} p_r^{(k-1)} \right)}{\sum_{m=1}^{n_d} l_{mj} + \frac{\sigma_d'^2}{\sigma_p^2 \Lambda}}. \tag{14}$$

We can assign Λ to the average length of the raypath in the case of slowness inversion or the average sum of partial derivatives in a general case:

$$\Lambda = \frac{1}{n_d} \sum_{m=1}^{n_d} L_m = \frac{1}{n_d} \sum_{m=1}^{n_d} \sum_{n=1}^{n_p} l_{mn}. \tag{15}$$

Using the above correspondence between the back-

projection tomography and the generalized inverse, we can relate the damping constant μ to the error in the data and the *a priori* error in the parameter by

$$\mu = \frac{\sigma_d'^2}{\sigma_p^2} \frac{n_d}{\sum_{m=1}^{n_d} \sum_{n=1}^{n_p} l_{mn}}. \tag{16}$$

If the data are not weighted by $1/L$, the expression of the damping factor is quite simple and is given by:

$$\mu = \frac{\sigma_d'^2}{\sigma_p^2}. \tag{17}$$

6 COMPARISON OF RESULTS IN CASE STUDIES

Results from the back-projection tomography have apparent spatial resolution of $6 \times 6 \times 2$ (or 1) km in the case of the

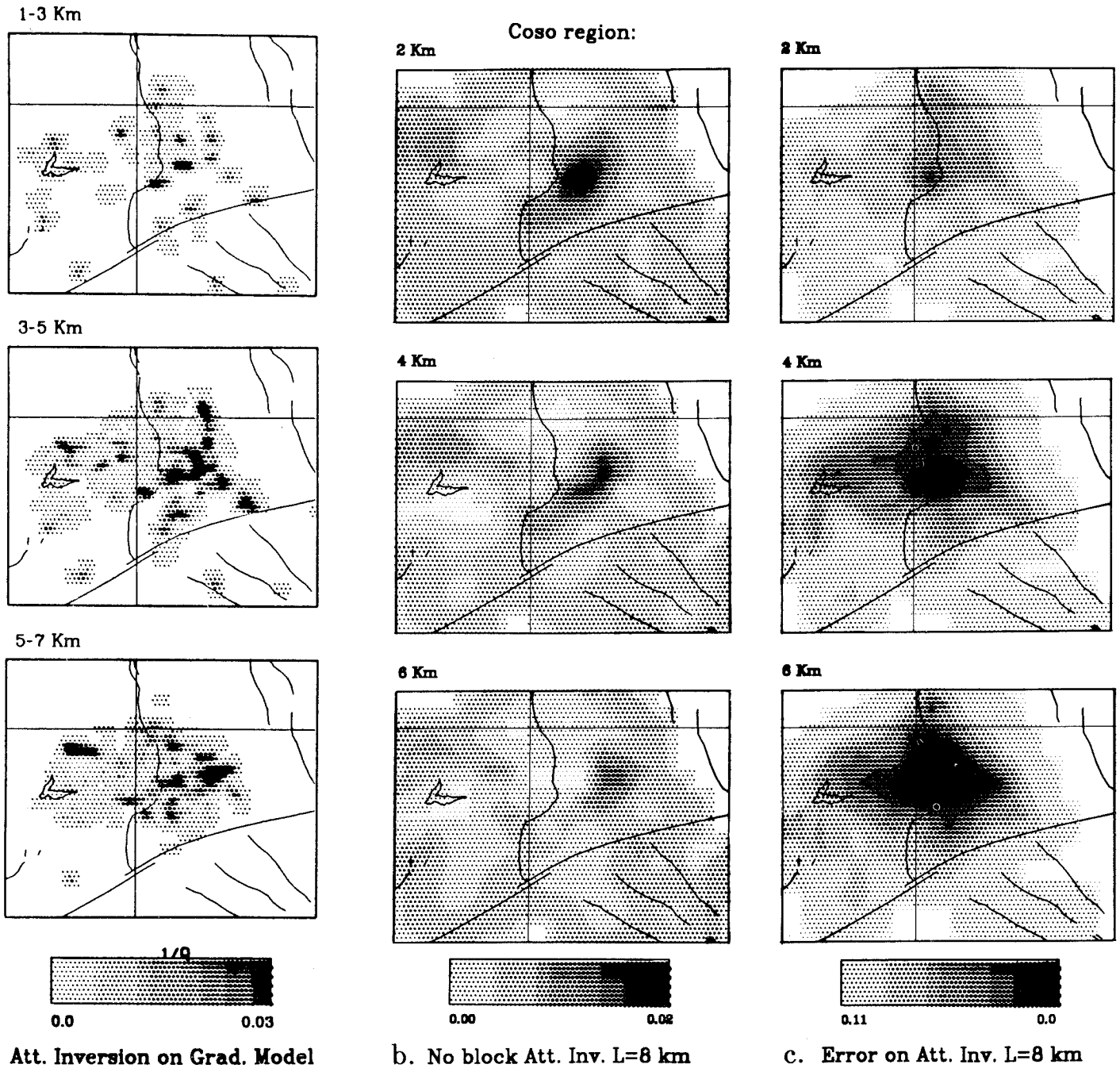

Figure 2. (a) Results of attenuation tomography using iterative back-projection method (Comer & Clayton 1987) on the Coso–Indian Wells region. Blocks sizes are $2 \times 2 \times 1$ km. Actual resolution is $6 \times 6 \times 1$ (or 2) km. Depth slices are shown in depths of 1–3 km, 3–5 km and 5–7 km. The major anomaly is the Indian Wells Valley anomaly east of the Sierra Nevada fault. (b) Results of attenuation tomography using no-block inversion technique (Tarantola & Valette 1982) in the Coso–Indian Wells region. The correlation length is 8 km, *a priori* error on Q is 100. Notice the similarity between the resolved anomaly and the Indian Wells Valley anomaly in 2(a). (c) Error on the results of attenuation tomography without blocks on Coso–Indian Wells region with correlation length of 8 km. Amplitude of error is smaller in the area where the major anomaly is located, suggesting that the major anomaly is well resolved.

Coso–Indian Wells region and $6 \times 6 \times 4$ km in the case of Imperial Valley. Hence, we compare the results from the no-block tomography with an L of 4 or 8 km. The empirical damping factor μ was chosen to be 30, based on the condition described by Comer & Clayton (1984). The value of σ_p was chosen to be 100 because, from equation (16), it corresponds to a damping factor of 30 used in the back-projection study.

Results from back-projection are shown in Figs 2(a), 3(a), 4(a) and 5(a). Blank areas are those crossed by less than two rays. Results from the no-block inversion are shown in Figs 2(b), 3(b), 4(b) and 5(b) for the Coso region and Imperial Valley, respectively. Figs 2(b) and 4(b) are for a correlation length of 8 km while Figs 3(b) and 5(b) are for a correlation length of 4 km.

The comparison between Figs 3(b) and 3(a) and between Figs 5(b) and 5(a) demonstrates that the results obtained by the two different methods are very similar. Locations of major anomalies are the same. The no-block technique tends to yield a rounded anomaly because of the *a priori*

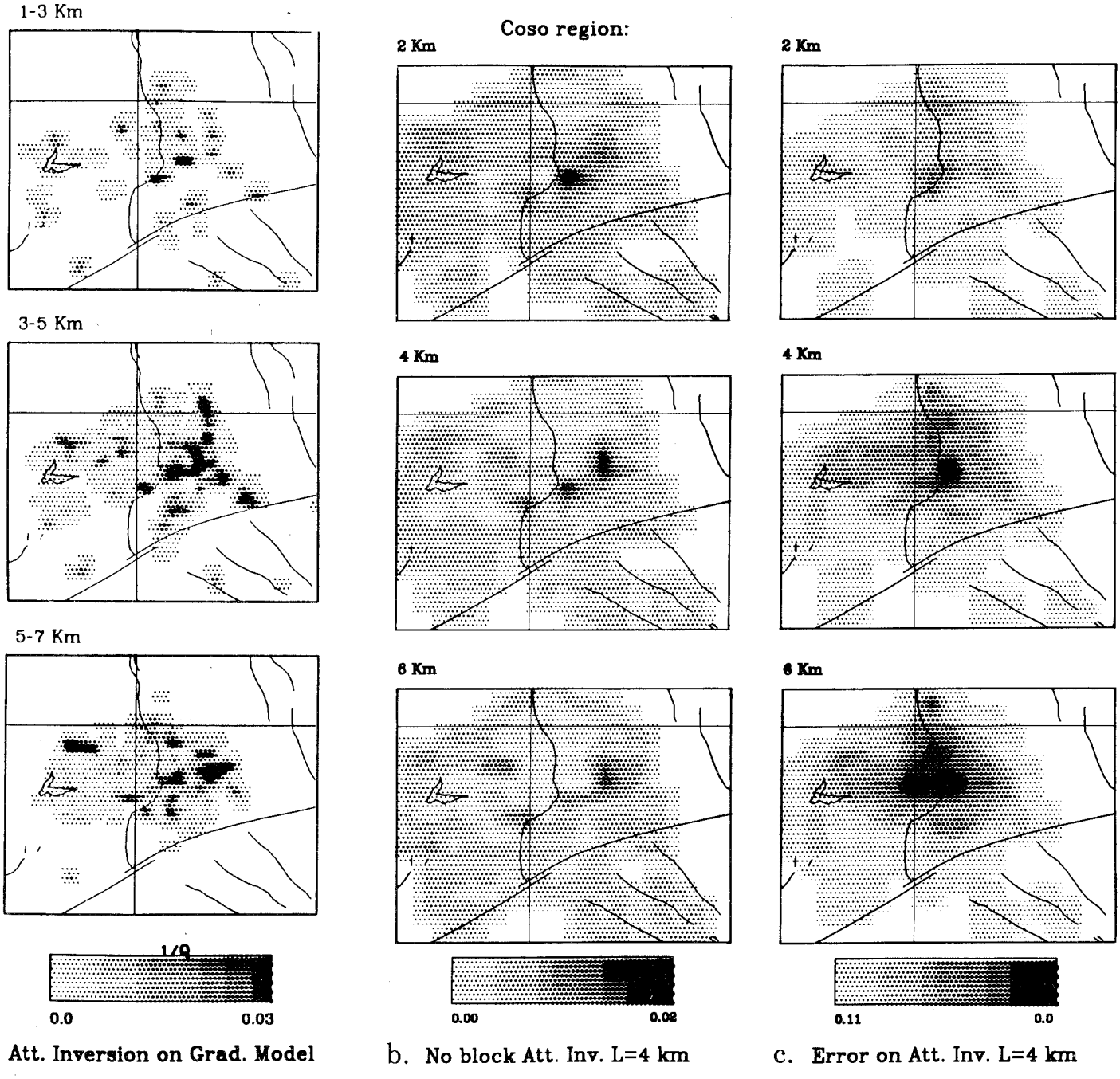

Figure 3. (a) Same results of attenuation tomography using iterative back-projection method (Comer & Clayton 1987) as in Fig. 2(a). (b) Results of attenuation tomography using no-block inversion technique (Tarantola & Valette 1982) in the same region. The correlation length is 4 km, *a priori* error on Q is 100. (c) Error on the results of attenuation tomography without blocks on Coso–Indian Wells region with correlation length of 4 km. Amplitude of error is also smaller in the area where the major anomaly is located, suggesting that the major anomaly is well resolved.

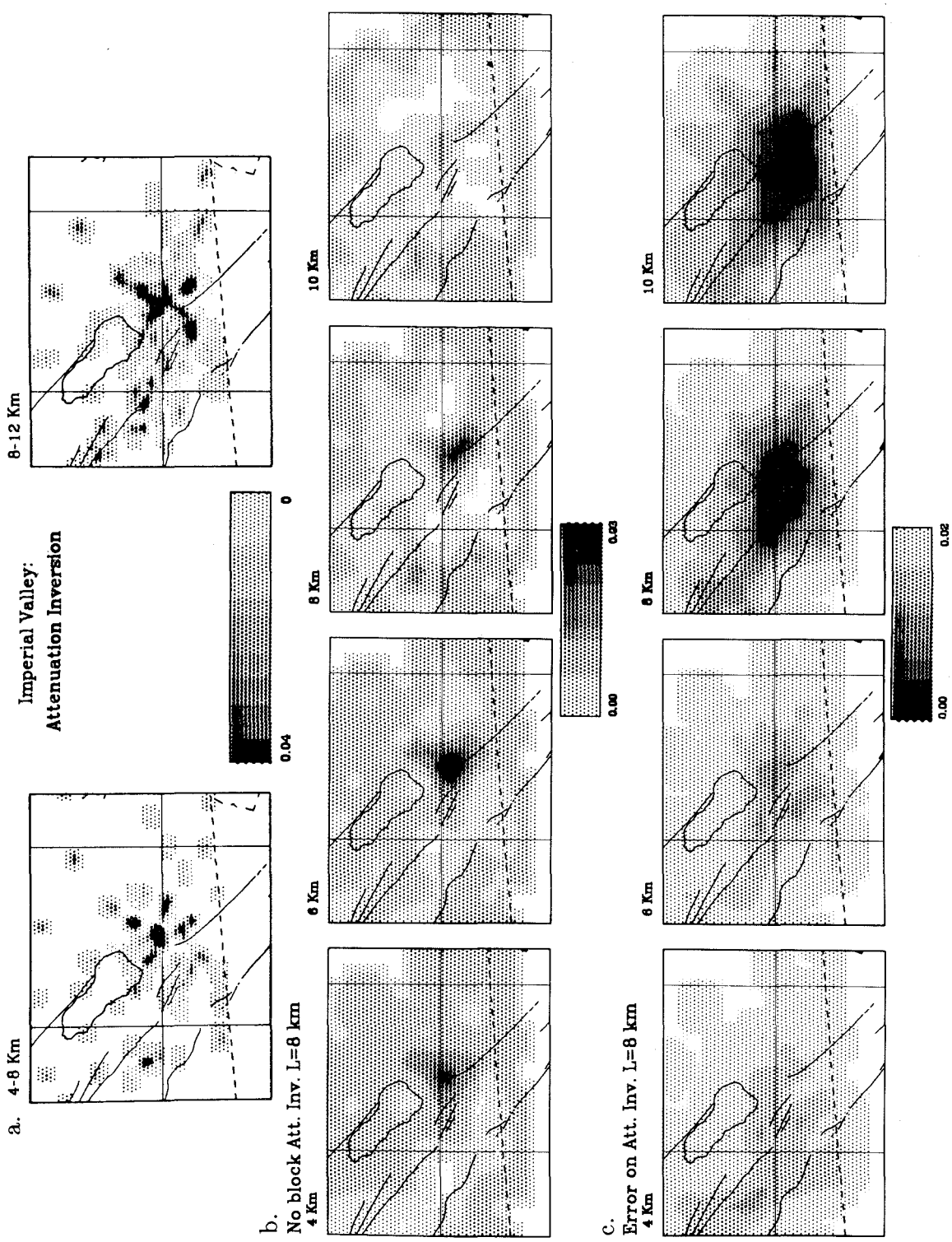

Figure 4. (a) Results of attenuation tomography using iterative back-projection method (Comer & Clayton 1987) on the Imperial Valley. Blocks sizes are $2 \times 2 \times 1$ km. Actual resolution is $6 \times 6 \times 4$ km. Depth slices are shown in depths of 4–8 and 8–12 km. The major anomaly is the Brawley anomaly north of the Imperial fault. (b) Results of attenuation tomography using no-block inversion technique (Tarantola & Valette 1982) in the Coso–Indian Wells region. The correlation length is 8 km, *a priori* error on Q is 100. The major anomaly at Brawley is also resolved. Note the similarities between the location of this anomaly and the location of the one resolved by iterative back-projection method shown in (a). (c) Error on the results of attenuation tomography without blocks on Imperial Valley with correlation length of 8 km. Amplitude of error is smaller in the area where the major anomaly is located, suggesting that the major anomaly is well resolved.

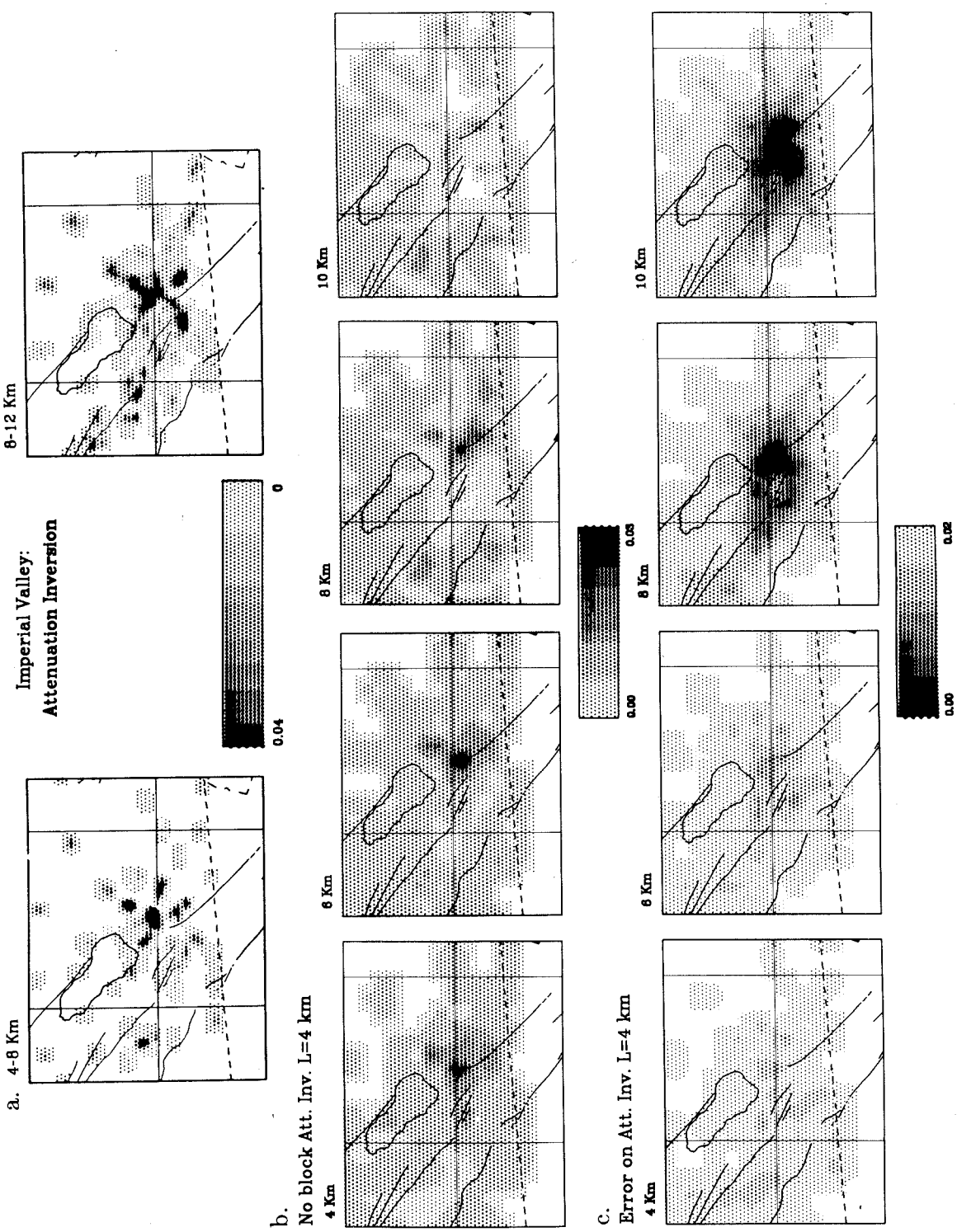

Figure 5. (a) Same results of attenuation tomography using iterative back-projection method (Comer & Clayton 1987) on the Imperial Valley as in Fig. 4(a). (b) Results of attenuation tomography using no-block inversion technique (Tarantola & Valette 1982) in the same region. The correlation length is 4 km, *a priori* error on Q is 100. The major anomaly at Brawley is also resolved. Due to the *a priori* assumption that the geometry of the anomaly is Gaussian in shape (see text for details), the shape of the anomaly is not as linear as in (a) but has two rounded anomalies at the two ends of the linear trend. (c) Error on the results of attenuation tomography without blocks on Imperial Valley with correlation length of 4 km. Amplitude of error is smaller in the area where the major anomaly is located, suggesting that the major anomaly is well resolved.

Gaussian covariance matrix. In the Coso case, since the anomaly resolved by iterative back-projection has a rounded shape, the shapes of the anomalies using both approaches are almost identical. The Imperial Valley anomaly resolved by the iterative back-projection method has a more linear trend. The no-block technique resolved two rounded anomalies at the two ends of the linear trend. In general, the results are very similar.

The model errors due to random data errors in the inversion can be calculated using equation (9a) and are shown in Figs 2(c) and 3(c) for Coso and 4(c) and 5(c) for Imperial Valley, respectively. The errors in the area where the anomalies are located are smaller than the anomaly, which means that at the locations of the anomalies, the anomalies are not due to random noise.

More details in the geometry of the anomalies are resolved with a smaller correlation length of 4 km, but the errors for the results with the anomalies are larger than those associated with a correlation length of 8 km [Figs 2(c) and 3(c) and Figs 4(c) and 5(c)]. By comparing results from these two approaches, we are confident that the locations and geometry of major anomalies in both cases are adequately resolved.

The results from the back-projection method indicate that the quality factor Q of the Coso anomaly is approximately 30, and that the Imperial Valley anomaly is approximately 20. From the no-block inversion technique with a correlation length of 8 km, we obtained a value of approximately 40 for Coso and 37 for Imperial Valley.

The resolution of a target point where the largest anomaly is located in each case is calculated using equation (9b). The closer the result is to a delta function, the better resolved the target point is. The resolutions at the locations of the anomalies in both cases are shown in Figs 6 and 7 for Coso and Imperial Valley cases at correlation length of 8 km. In the case of Coso, the target point at which resolution is calculated is at 4 km depth and the resolution calculation has its maximum at 4 km in a form close to a delta function (Fig 6), demonstrating that the anomaly is correctly located. In the Imperial Valley, the target point is situated at 6 km, but the resolution calculation puts the maximum at 8 km depth (Fig. 7), where the error is smaller than at 6 km depth (Fig. 4c),

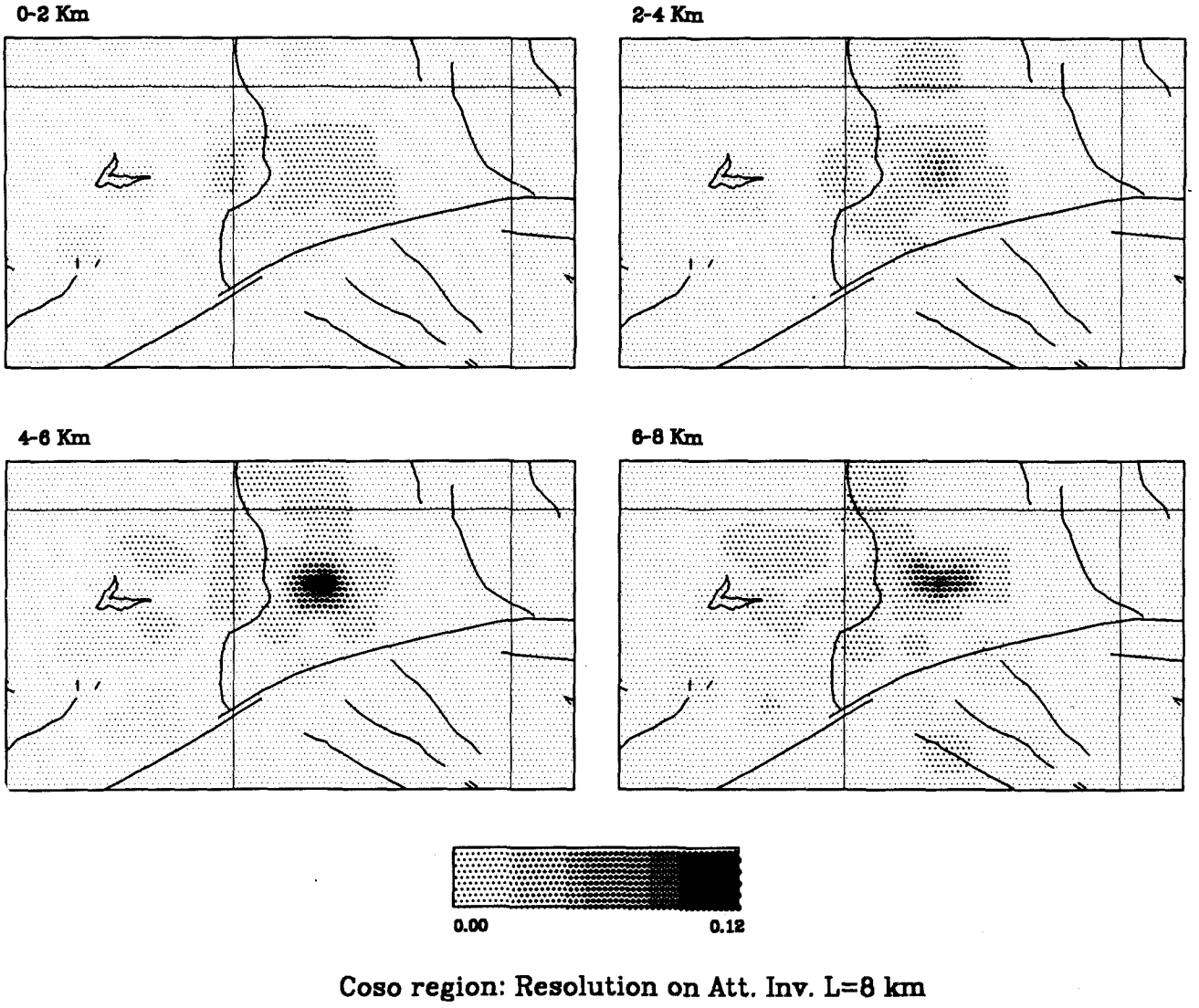

Figure 6. Resolution at the location of the Indian Wells Valley anomaly is shown in depth slices. The resolution is better if the result is more 'point-like'. We can see that this is the case for this correlation length of 8 km.

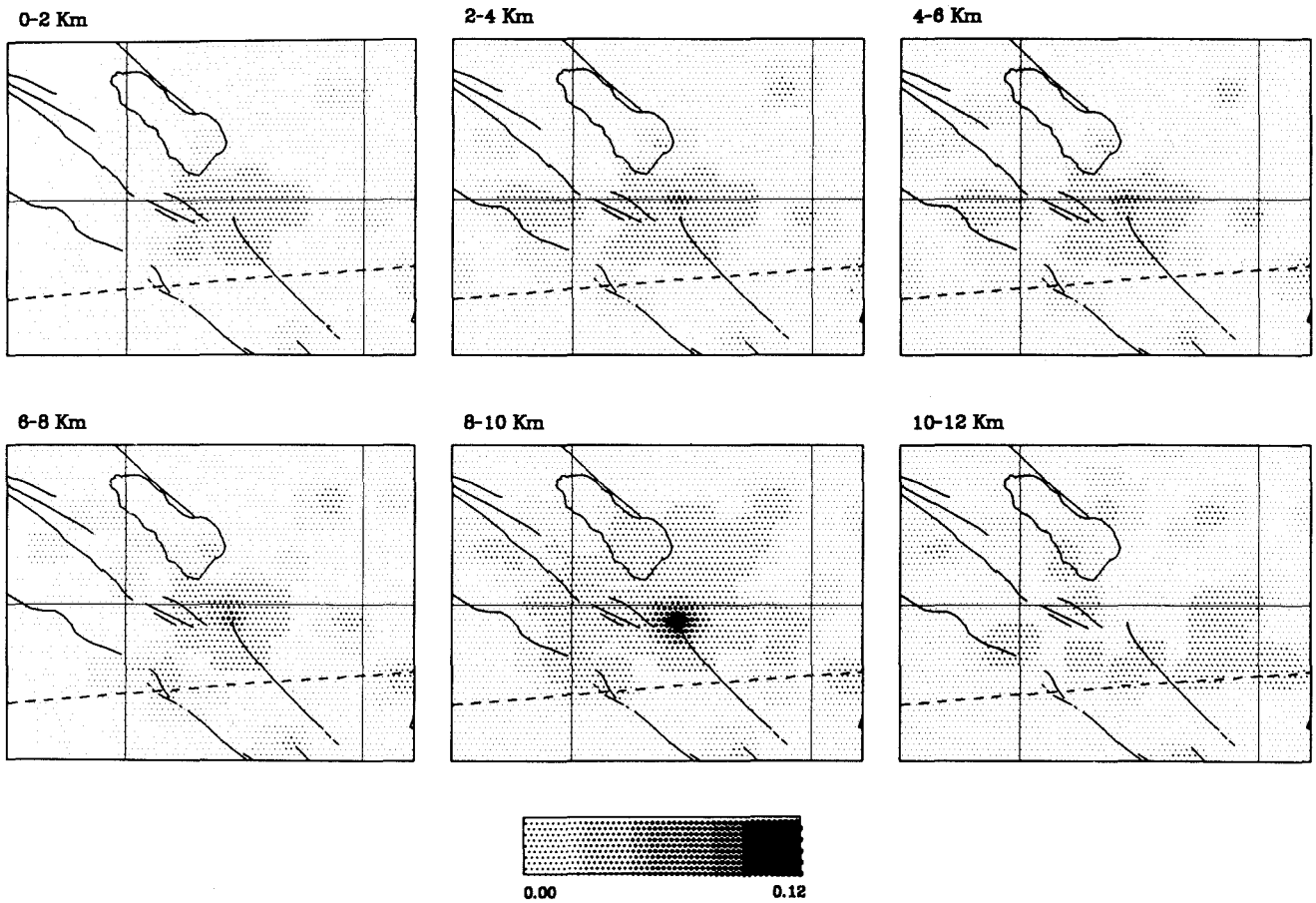

Figure 7. Resolution at the location of the Brawley anomaly is shown in this figure. Again the result shows a very point-like resolution at the location of the anomaly, implying good resolution at this location. The target point is situated at 6 km, and the resolution maximum is at 8 km where the error is smaller (see Fig. 4c), as a result of the trade-off between resolution and error. So we expect resolution in the depth of the anomaly carries an error range of about 2 km in depth.

suggesting a possible 2 km error in the depth of the resolved anomaly. The overall pattern on a map view, however, remains deltalike, which suggests that the resolved geometry of the anomaly is adequate.

7 DISCUSSION AND CONCLUSION

We have presented a direct comparison between two different inversion techniques: back-projection and no-block inversion. The results of inversion obtained by these two methods are very similar. Comparison of the results obtained by these two methods allows direct interpretation and investigation of the errors, resolution, and the choice of damping factor in the back-projection technique.

The back-projection technique is a more direct approach to the problem, but errors and resolution can be only indirectly estimated. It is more computationally efficient, for example, for the problems shown in this paper, 30 iterations take approximately 1.5 h on a VAX 11/780.

The no-block inversion technique is a more generalized approach, making use of *a priori* knowledge or assumption on the parameters and data. Resolution is governed not only by the path coverage, but also by the *a priori* model covariance function (where the correlation length L defines the width of any resolved anomaly). By adjusting the covariance function, it is possible to look for the model explaining the data set with a desired resolution. Error estimates can be directly computed from the final model, assuming an *a priori* estimate of errors. Computationally, it is more expensive, requiring more than 5 h on a VAX 11/780.

ACKNOWLEDGMENTS

We thank Don Anderson and Jiajun Zhang for reviewing the manuscript. Discussions with Rob Clayton have been very helpful. This work was supported by USGS Grant 14-08-0001-G1171. Contribution number 4572 from Division of Geological and Planetary Sciences, California Institute of Technology.

REFERENCES

Aki, K. & Lee, W. H. K., 1976. Determination of three-dimensional velocity anomalies under a seismic array using first P arrival times from local earthquakes, 1. A homogeneous initial model, *J. geophys. Res.*, **81**, 4381–4399.

Backus, G. & Gilbert, F., 1968. The resolving power of gross earth data, *Geophys. J.R. astr. Soc.*, **16,** 169–205.

Backus, G. & Gilbert, F., 1970. Uniqueness in the inversion of inaccurate gross earth data, *Phil. Trans. R. Soc. A*, **266,** 123–192.

Chou, W. C. & Booker, R. J., 1979. A Backus–Gilbert approach to inversion of travel-time data for three-dimensional velocity structure, *Geophys. J.R. astr. Soc.*, **59,** 325–344.

Clayton, R. W., 1984. Seismic tomography, *Eos, Trans. Am. Geophys. Un.*, **65,** 236.

Comer, R. P. & Clayton, R. W., 1984. Tomographic reconstruction of lateral velocity heterogeneity in the Earth's mantle, *EOS*, **65,** 236.

Dines, K. A. & Lytle, R. J., 1979. Computerized geophysical tomography, *Proc. IEEE*, **67,** 1065–1073, 1979.

Franklin, J. N., 1970. Well-posed stochastic extensions of ill-posed linear problems, *J. math. Anal. Appl.*, **31,** 682–716.

Hearn, T. M. & Clayton, R. W., 1986a. Lateral velocity variations in southern California: 1. Results for the upper crust from Pg-waves, *Bull. seism. Soc. Am.*, **76,** 511–520.

Hearn, T. M. & Clayton, R. W., 1986b. Lateral velocity variations in southern California: 2. Results for the lower crust from *Pn*-waves, *Bull. seism. Soc. Am.*, **76,** 495–509.

Ho-Liu, P., Kanamori, H. & Clayton, R. W., 1988. Applications of attenuation tomography to Imperial Valley and Coso-Indian Wells region, southern California, *J. geophys. Res.*, **93,** 10501–10520.

Jackson, D. D., 1979. The use of *a priori* data to resolve non-uniqueness in linear inversion, *Geophys. J. R. astr. Soc.*, **57,** 137–157.

Nercessian, A., Hirn, A. & Tarantola, A., 1984. Three-dimensional seismic transmission prospecting of the Mont Dore volcano, France, *Geophys. J. R. astr. Soc.*, **76,** 307–315.

Tarantola, A. & Valette, B. 1982. Generalized nonlinear inverse problems solved using the least squares criterion, *Rev. Geophys. Space Phys.*, **20,** 219–232.

Tarantola, A. & Nercessian, A. 1984. Three-dimensional inversion without blocks, *Geophys. J. R. astr. Soc.*, **76,** 299–306.

Walck, M. C., 1988. Three-dimensional V_p/V_s variations for the Coso region, California, *J. geophys. Res.*, **93,** 2047–2052.

Walck, M. C. & Clayton, R. W. 1988. *P*-wave velocity variations in the Coso region, California, derived from local earthquake travel times, *J. geophys. Res.*, **92,** 393–406.

Wiggins, R. A., 1972. The general inverse problem: implications of surface waves and free oscillations for earth structure, *Rev. Geophys. Space Phys.*, **10,** 251–285.